SANDIA REPORT

SAND2003-8586
Unlimited Release
Printed November 2003

Oxide Dispersion Strengthening of Nickel Electrodeposits for Microsystem Applications

S. H. Goods, T. E. Buchheit, R. P. Michael,
P.G. Kotula, R. P. Janek

Prepared by
Sandia National Laboratories
Albuquerque, New Mexico 87185 and Livermore, California 94550

Sandia is a multiprogram laboratory operated by Sandia Corporation,
a Lockheed Martin Company, for the United States Department of Energy's
National Nuclear Security Administration under Contract DE-AC04-94AL85000.

Sandia National Laboratories

Issued by Sandia National Laboratories, operated for the United States Department of Energy by Sandia Corporation.

Available to DOE and DOE contractors from
U.S. Department of Energy
Office of Scientific and Technical Information
P.O. Box 62
Oak Ridge, TN 37831

Telephone: (865)576-8401
Facsimile: (865)576-5728
E-Mail: reports@adonis.osti.gov
Online ordering: http://www.osti.gov/bridge

Available to the public from
U.S. Department of Commerce
National Technical Information Service
5285 Port Royal Rd
Springfield, VA 22161

Telephone: (800)553-6847
Facsimile: (703)605-6900
E-Mail: orders@ntis.fedworld.gov
Online order: http://www.ntis.gov/help/ordermethods.asp?loc=7-4-0#online

SAND2003-8586
Unlimited Release
Printed November 2003

Oxide Dispersion Strengthening of Nickel Electrodeposits for Microsystem Applications

S. H. Goods
Sandia National Laboratories,
Livermore, CA 94550

T. E. Buchheit, R. P. Michael, P.G. Kotula
Sandia National Laboratories
Albuquerque, NM 87185
and
R. P. Janek,
Owens Technology Inc.,
Palo Alto, CA 94306

Abstract

Oxide dispersion strengthened nickel (ODS-Ni) electrodeposits were fabricated to net shape in a nickel sulfamate bath using the LIGA process. A 20 g/l charge of 10 nm Al_2O_3 powder was suspended in the bath during electrodeposition to produce specimens containing an approximately 0.001-0.02 volume fraction dispersion of the alumina particulate. Mechanical properties are compared to baseline specimens fabricated using an identical sulfamate bath chemistry without the Al_2O_3 powder charge. Results reveal that the as-deposited ODS-Ni exhibited significantly higher yield strength and ultimate tensile strength than the baseline material. This increase in as-deposited strength is attributed to Orowan strengthening. The ODS-Ni also showed improved retention of room temperature strength after annealing over a range of temperatures up to 600 °C. Microscopy revealed that this resistance to anneal softening was due to an inhibition of grain growth in the presence of the oxide dispersion. Nanoindentation measurements revealed that the properties of the dispersion strengthened deposit were uniform through its thickness, even in narrow, high aspect ratio structures. At elevated temperatures, the strength of the ODS-Ni was approximately three times greater than that of the baseline material although with a significant reduction in hot ductility.

Acknowledgments

The authors gratefully acknowledge the assistance of D. Schmale in the gathering of the mechanical test data. We thank C. Cadden and B. Boyce for their critical review of this manuscript. Sandia is a multi-program laboratory operated by Sandia Corporation, a Lockheed Martin Company, for the United States Department of Energy under Contract DE-AC04-94AL85000.

Contents

List of Figures

List of Tables

I. Introduction

Electrodeposition of metals in thick polymethylmethacrylate (PMMA) or SU-8 photoresist molds has enabled the fabrication of high aspect ratio microstructures, *i.e.* large height to width ratio, for various microsystems applications.[1-5] Electrodeposited microsystem components afford the possibility of the design, fabrication and assembly of mechanical and electromechanical devices at a size scale that is smaller than that achievable through conventional small scale machining. These metallic components have higher toughness than those realized through silicon surface micromachining. In many cases, individual components of a microsystem device will function as a spring or flexure and therefore the structural materials used will be required to have specific pre-defined mechanical properties. As the cross-sectional areas of these load-bearing components decrease (to save space and weight, for example), the stresses they experience necessarily increase,[6] often requiring the use of exceptionally high strength materials.

The current study is directed toward realizing enhanced mechanical properties in through-thickness mold electrodeposits for high aspect ratio microsystem (HARMS) applications, in particular, the LIGA process. LIGA is an acronym derived from the German words: *Lithographie, Galvanoformung, Abformung* (Lithography, Electroforming, Molding). The direct version of this process is capable of producing discrete, free-standing metallic parts with lateral dimensions ranging from ~10 μm to 1-2 cm and thicknesses usually on the order of 100s of microns but potentially as thick as several millimeters. The process begins by exposing a wafer assembly (composed of a patterned X-ray lithography mask and a photoresist blank bonded to a conductive substrate) to X-ray synchrotron radiation. The typical photoresist is PMMA and the common substrate materials are metallized glass or a metallized silicon wafer. X-ray radiation renders the exposed portions of the PMMA susceptible to dissolution by an appropriate chemical developer permitting development of a mold consisting of deep vertical cavity features with geometric tolerances on the order of 1 μm. The mold is then immersed in an electroplating bath and the cavities are filled with an electrodeposited metal or alloy. Subsequent processing steps involve planarization of the top surface, removal of the PMMA and chemical release of the final piece parts.

Constraints resulting from through-mold deposition usually reduce the choice of electrodeposit to either copper or nickel which, as elemental metals, deposit easily but do not have sufficient strength in the as-deposited condition for certain applications. Also, these pure metal electrodeposits anneal soften readily. As a result, much work has been directed towards increasing the strength and resistance to anneal softening of candidate electrodeposited materials for HARMS applications, in particular nickel-based electrodeposits.[7-11] One approach is to incorporate an organic additive such as

saccharin in the plating bath to refine the grain size.[7] In this case, sulfur from the saccharin additive dramatically reduces the grain size to the range of 10s to 100s nm with an associated dramatic increase in tensile strength to values approaching 1600 - 1800 MPa. While this approach successfully increases strength, incorporation of sulfur may reduce ductility [9] or bring with it the potential for catastrophic embrittlement when deposits are subjected to elevated temperatures ($\geq$ 300°C).[7,9,10] Furthermore, grain refinement by way of incorporating the sulfur bearing additive into an electrodeposit does not promote resistance to anneal softening.

Some higher strength binary alloys, such as Ni-Fe and Ni-Co, are readily electrodeposited as thin sheets or surface films. In these cases, the increase in strength relative to pure metal electrodeposits arises primarily from refined grain morphologies. However, constraints arising from through-mold deposition limit the choice of practical material systems. For example, nickel-cobalt alloys can be electrodeposited at cobalt concentrations as high as 60%.[7] This alloy system has a very small average grain size (approx. 200-400 nm) and can exhibit yield strengths as high as 1600 MPa while maintaining good ductility. However, the electrodeposition characteristics of cobalt relative to nickel invariably results in a severe gradient in cobalt content and non-uniform mechanical properties in through-mold deposits. Even in alloy systems where the compositional variation is less extreme, elevated plating stresses compromise the ability to successfully plate in thick sections[11] and the integrity and quality of final parts. From a practical perspective, few, if any, binary alloys have been found suitable for through mold deposition applications.

An alternative approach to developing high strength electrodeposits, and in materials in general, is to physically incorporate an inert, hard particulate dispersoid, typically an oxide such as alumina (Al_2O_3), into the host metal matrix, creating a particulate composite. The source of the strength increase is the Orowan hardening phenomena wherein the distributed particulates act as barriers to dislocation motion within the metal matrix.[12,13] An additional benefit may be realized if the particulate microstructure acts to pin the grain boundaries thereby impeding grain growth during heat treatment. If so, the particulate composite may exhibit resistance to grain growth-based anneal softening. The ability to successfully co-deposit a particulate in both thin and thick electrodeposited films has been previously demonstrated [14-19] and the volume fraction of the incorporated particulate can be varied by adjusting the current density.[20,21]

This article examines the potential for through-mold deposition of oxide dispersion strengthened nickel (ODS-Ni) as a particulate composite for microsystem applications by comparing its microstructure and properties to baseline electrodeposited nickel. Both materials were fabricated by electrodeposition from a sulfamate bath chemistry.

The only difference between baseline Ni and ODS-Ni deposition baths was the addition of 10 nm (diameter) Al_2O_3 powder to the electrolyte solution prior to fabrication of the ODS Ni samples. Mechanical test specimens were fabricated from both baths and used to characterize the extent of strengthening and the decreased susceptibility to anneal softening when the ODS agent was incorporated into the samples. The uniformity in the mechanical properties of the electrodeposited structures was assessed via nanoindentation surveys through the thickness of the deposits. To complete the study and understand the role of the strengthening agent, electron microscopy was used for comparative characterization of the grain size, grain morphology and the particle distribution in as-deposited and annealed samples.

II. Experimental

Specimen preparation and testing

Net shape tensile specimens were fabricated using the LIGA process as described above. Bath composition and deposition conditions used in this study are given in Table I. Baseline, particulate-free, Ni specimens were deposited from a sulfamate bath chemistry.

Table I: Plating Bath Composition and Deposition Conditions

Ni-Sulfamate, $[Ni(SO_3)_2]$	1.25 M
Boric Acid, $[H_2BO_3]$	0.5 M
SDS[a] (surfactant)	0.2 g/l
pH	4.1
Temperature	50 °C
Current density	20 mA/cm^2
----------	----------
0.01 μm Al_2O_3 Degussa	20 g/l

[a] sodium dodecyl sulfate

The ODS-Ni specimens were deposited using an identical sulfamate bath chemistry charged with 20g/l of Al_2O_3 powder. The powder was obtained from Degussa, AG and had a mean particle diameter of ~10 nm. It was kept suspended in the bath through vigorous stirring throughout the deposition process. After final planarization and release from the substrate, mechanical test specimens fabricated from both baseline Ni and ODS-Ni baths were tested in tension using a custom built tabletop servohydraulic test frame. The LIGA fabricated tensile specimens had a gage length of 3.08 mm and measured

0.76 mm wide by approximately 0.3 mm in thickness. Load was measured using a 450 N Sensotec load cell and strain was measured using a Keyence non-contacting laser micrometer. Complete descriptions of the testing apparatus and specimen geometry are available elsewhere.[22,23] Baseline and ODS-Ni specimens were tested in the as-plated condition at room temperature. To study the effects of heat treating, specimens were tested at room temperature and after one hour vacuum annealing treatments at: 200 °C, 300 °C, 400 °C, 500 °C and 600 °C. Finally, specimens were tested at three elevated temperatures, 300 °C, 400 °C and 500 °C, to examine the influence of the dispersoid on high temperature properties. All testing was performed at a constant extension rate of 5.5 x 10^{-3} mm/sec, corresponding to an initial strain rate of ~1 x 10^{-3} sec^{-1}. For the most ductile specimens, testing was terminated after a total imposed strain of ~ 30%.

An MTS Nanoindenter (Model XP) was used to characterize the uniformity of the deposits with respect to hardness and strength. Instrumented indentation measurements were performed on metallographically prepared through-mold electrodeposit cross-sections. These measurements were correlated with the yield strength of the electrodeposited material, obtained using the LIGA fabricated tensile specimens, and compared with a previous correlation to the measured yield strength of similar electrodeposited materials.[23]. In the present work, measurements were performed on both low aspect ratio (1:10), bulk materials and high aspect ratio (10:1) features in order to assure that transport limitations (of the Al_2O_3 particulate) did not compromise the uniformity of the deposits in the most narrow features.

Microstructural characterization

Focused ion beam (FIB), scanning electron microscopy (SEM) and transmission electron microscopy (TEM) were used to characterize the microstructure of as-deposited and heat treated samples. One extremely useful grain structure imaging technique was ion beam induced channeling contrast imaging in the FIB instrument.[24] An FEI DB235 dual beam FIB, producing 30kV Ga^+ ions, was used to create channeling contrast images by scanning the ion beam over the region of interest on a metallographically prepared sample. The depth of penetration of the ions is related to the crystallographic orientation of the grain. Certain crystallographic orientations result in stronger ion channeling and therefore deeper penetration of the ions into the sample. Deeper ion penetration produces fewer collectable secondary electrons, so strongly channeling orientations appear dark as compared to more weakly channeling orientations. The amount of channeling is quite sensitive to small variations (1-2 degrees) in orientation so that not only can grains of different orientations be imaged, but small misorientations within a grain can be visualized as well.

The FIB system was also used to extract thin samples for observation in TEM. The samples were produced using standard FIB-based techniques and then were transferred to carbon coated support grids.[25] Transmission Electron Microscopy (TEM) and TEM-based X-ray spectral imaging using a FEI electron optics Tecnai F30-ST microscope were used to characterize local particle distributions, focusing on characterizing the degree of clustering of the fine-scale particles are within the FIB prepared samples.

III. Results

Mechanical Properties at Room Temperature

Figure 1(a) shows representative stress-strain curves for the room temperature behavior of the baseline Ni specimens in the as-deposited and heat treated conditions. The yield strength of the as-deposited samples is approximately 410 MPa while the ultimate tensile strength (UTS) is approximately 620 MPa. Engineering strain to failure of the as-deposited material is approximately 13%. These values are in general agreement for Ni-sulfamate films deposited under the conditions identified in Table I.[7] For the annealed samples, softening begins to occur between 200 °C and 300 °C (about 0.3 T_M), temperatures typically associated with recovery processes for Ni. Upon annealing at 600 °C for one hour the yield strength falls to 145 MPa while the UTS is 400 MPa. The ductility for specimens annealed at temperature ≥ 400 °C is in excess of 30%. Yield and UTS data are summarized in Figure 1(b) and in Table II. Each value represents the average of two measurements.

Table II: Average Room Temperature Mechanical Properties

Annealing Temperature (°C)	Yield Strength (MPa)		UTS (MPa)	
	Baseline	ODS	Baseline	ODS
As-Deposited	410	640	620	960
200	455	700	630	930
300	395	595	545	935
400	245	615	445	905
500	205	635	434	870
600	145	585	400	815

Figure 2(a) shows the room temperature stress-strain behavior of representative as-deposited and heat treated ODS-Ni specimens. For these specimens, the room temperature yield strength average 640 MPa while the UTS is approximately 960 MPa. These values represent an increase in both yield strength and UTS of ~ 50% with respect to the as-deposited baseline Ni. A loss in ductility is observed when the ODS-Ni

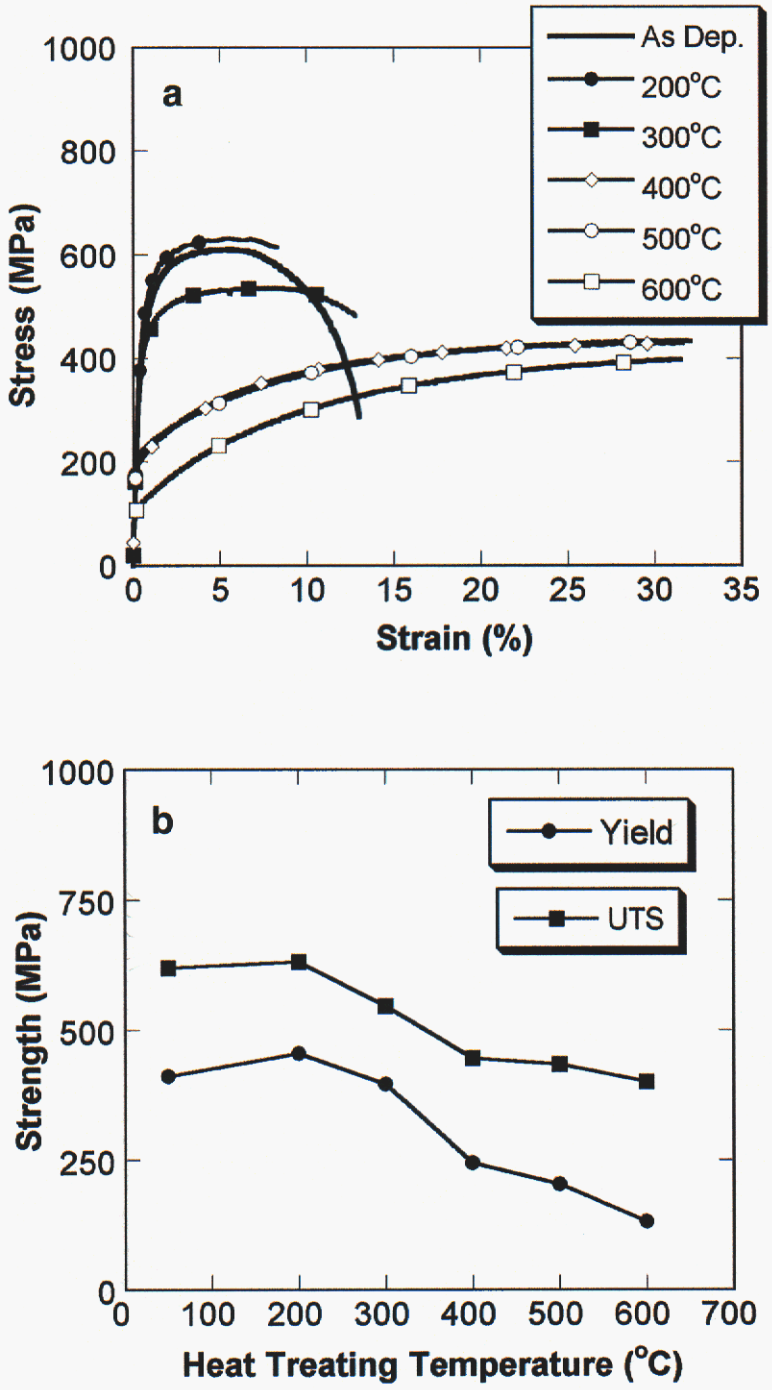

Figure 1. (a) Room temperature stress-strain curves for baseline Ni samples, electrodeposited from a sulfamate bath chemistry, in the as-deposited condition and after 1 hour heat treatments at temperatures between 200 °C and 600 °C. (b) Dependence of the room temperature yield strength and UTS on heat treatment temperature for baseline nickel.

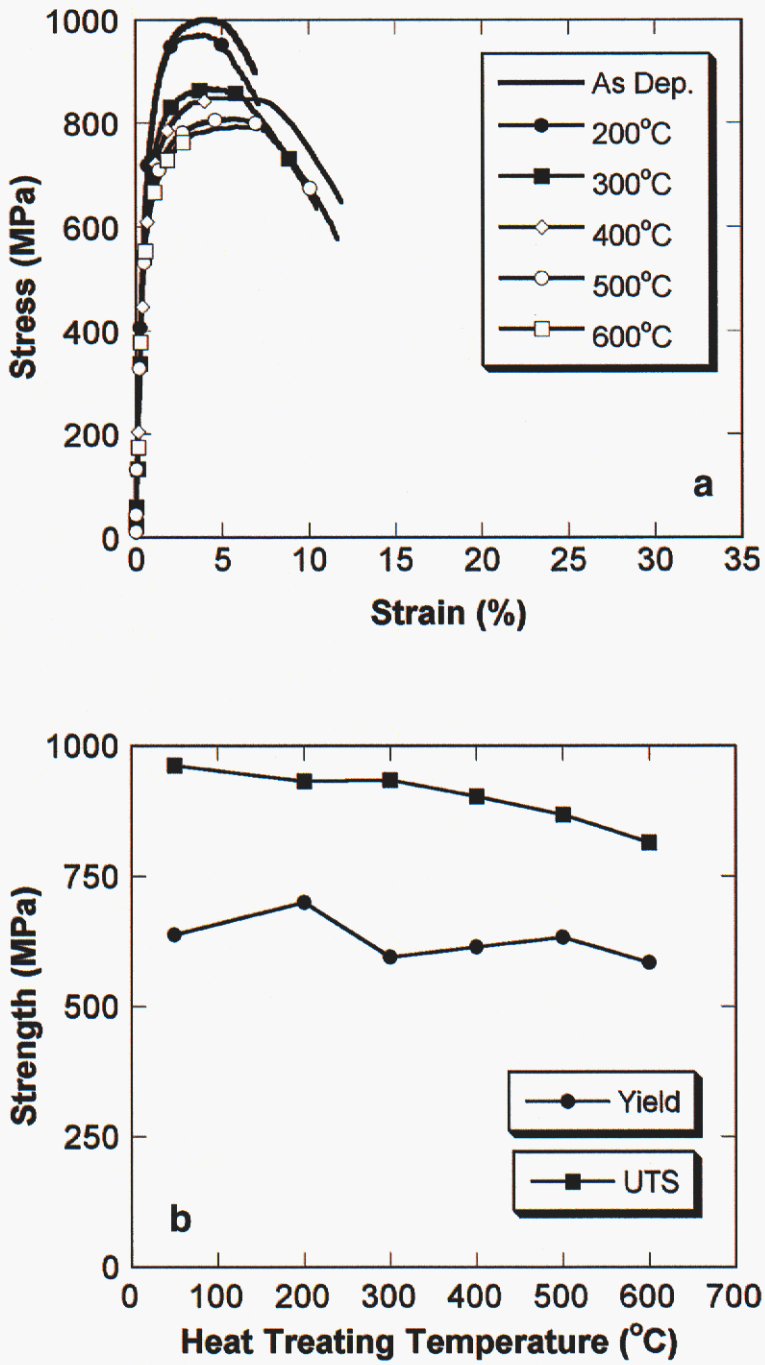

Figure 2. (a) Room temperature stress-strain curves for ODS-Ni samples in the as-deposited condition and after 1 hour heat treatments at temperatures between 200 °C and 600 °C. (b) Dependence of the room temperature yield strength and UTS on heat treatment temperature for ODS-Ni.

results are compared with the baseline nickel results, with strain to failure decreasing to ~ 7%. Upon heat treating, both the yield and ultimate strengths decrease in ODS-Ni samples, but to a far lesser extent than the baseline specimens. Subsequent to annealing at 600 °C, the yield strength of the ODS-Ni specimens is 585 MPa and the UTS is 815 MPa. These represent only a 9% and 15% decrease in yield and UTS respectively. Ductility only marginally increases to ~ 9.5%. Yield and UTS data for the ODS specimens are summarized over the entire annealing range in Figure 2(b) and in Table II. To emphasize the influence of the dispersoid on the increased as-deposited strength and on strength retention after annealing, Figure 3 directly compares stress-strain results of the as-deposited baseline Ni and ODS-Ni samples [Figure 3(a)] and after annealing at 600 °C for 1 hr [Figure 3(b)]. The considerable effect of the dispersoid on as-deposited strength and ductility, and on strength retention after annealing is clearly illustrated in this figure.

Figures 4(a) and 4(b) illustrates percentage changes in strength relative to the as-deposited material as a function of annealing temperature where:

$$\Delta\sigma = -100 \times \left(\frac{\sigma_{As-Dep} - \sigma_{Temp}}{\sigma_{As-Dep}} \right) \qquad (1)$$

This figure clearly shows the effect of the oxide dispersoid on strength over the entire range of annealing temperatures considered in this study. Between 300 °C and 400 °C there is a precipitous loss in strength of the baseline Ni. Strength continues to decrease with increasing annealing temperature and the average loss in yield strength for the baseline Ni specimens tested after the 600 °C annealing treatment is nearly 65%. For ODS-Ni, no such drop is evident between 300 °C and 400 °C and the average loss in yield strength is only about 10% after annealing at 600 °C.

Mechanical properties at elevated temperature

The ODS-Ni continued to show enhanced strength even at elevated temperatures. Figures 5(a) and 5(b) show stress-strain curves for baseline Ni and the ODS-Ni tested at the temperatures indicated. The baseline Ni sulfamate deposit shows a reduction in yield strength from 410 MPa in the as-deposited condition to 100 MPa when tested at 500 °C, while the UTS falls from 620 MPa to 165 MPa. These decreases represent an approximately 75% loss in strength. By contrast, the ODS deposit suffered a 50% loss in yield strength and 65% loss in UTS. More importantly, the yield strength of the ODS-Ni is three times higher than that of the baseline Ni at elevated temperature while its UTS is twice as high. Table III summarizes the elevated temperature strength of both the baseline and ODS-Ni. High temperature ductility of the ODS-Ni is, however, severely compromised as is evident from Figure 5(b). At the higher test temperatures, strain to failure of the ODS-Ni is less than 2%.

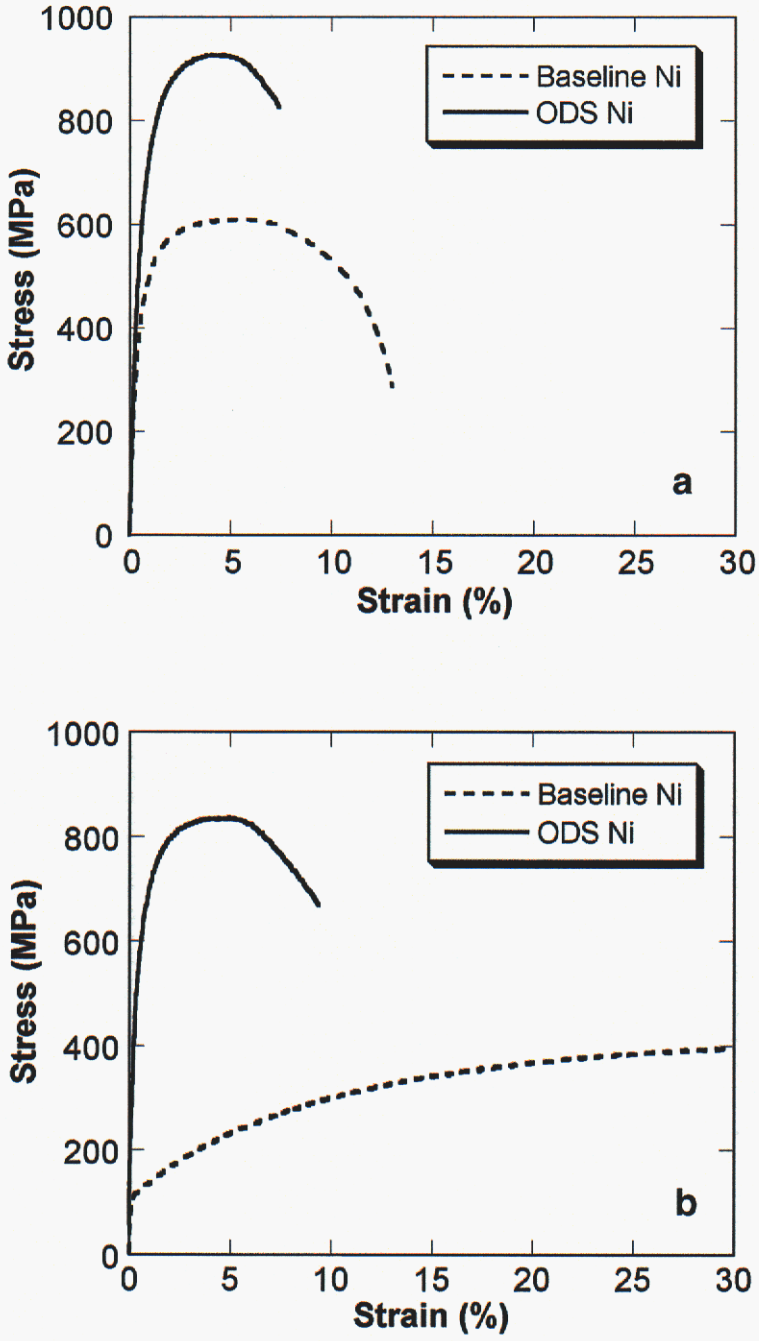

Figure 3. Comparison of the stress-strain response at room temperature of: (a) as-deposited samples and (b) samples heat treated at 600 °C for 1 hour.

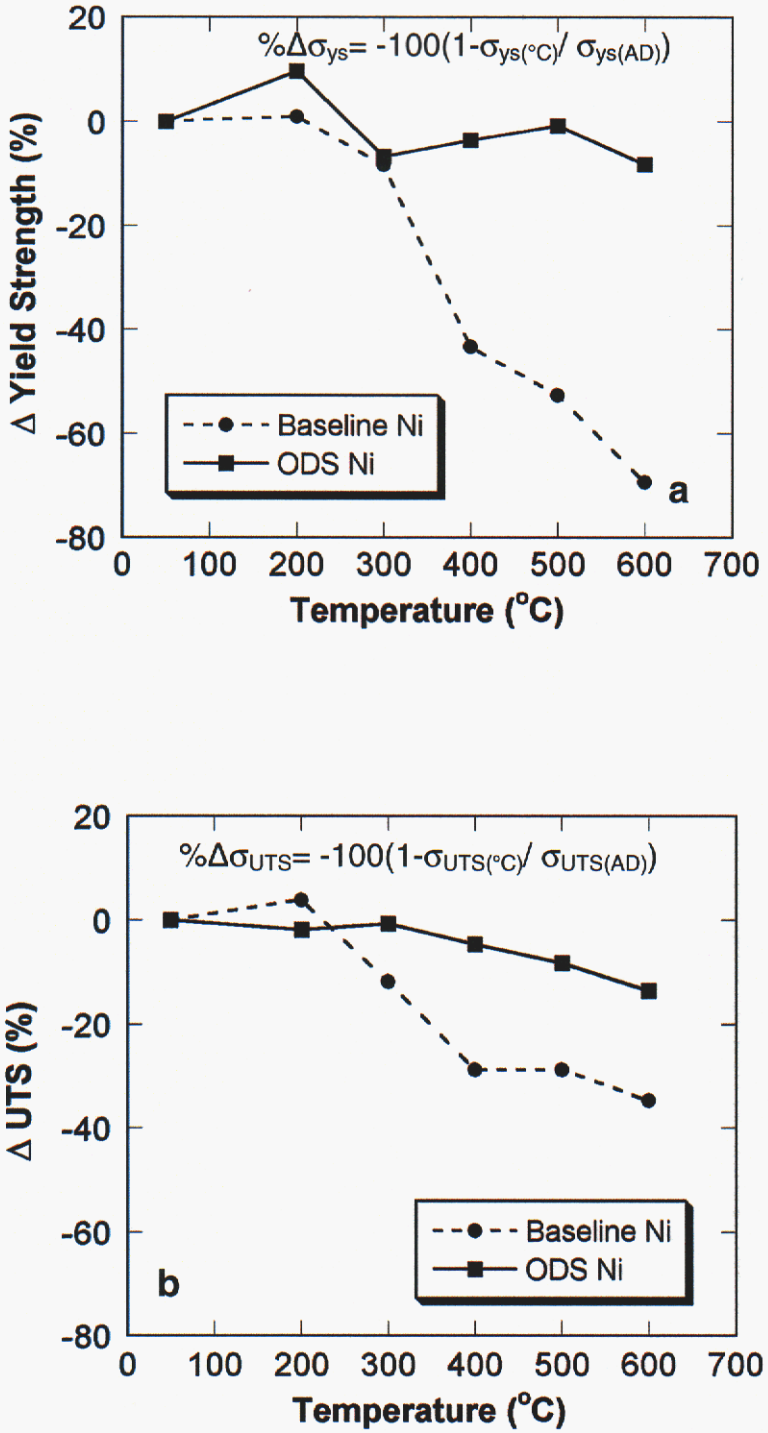

Figure 4. Percent decrease in (a) room temperature yield strength and (b) room temperature UTS after 1 hour heat tYeatments at temperatures between 200 °C and 600 °C.

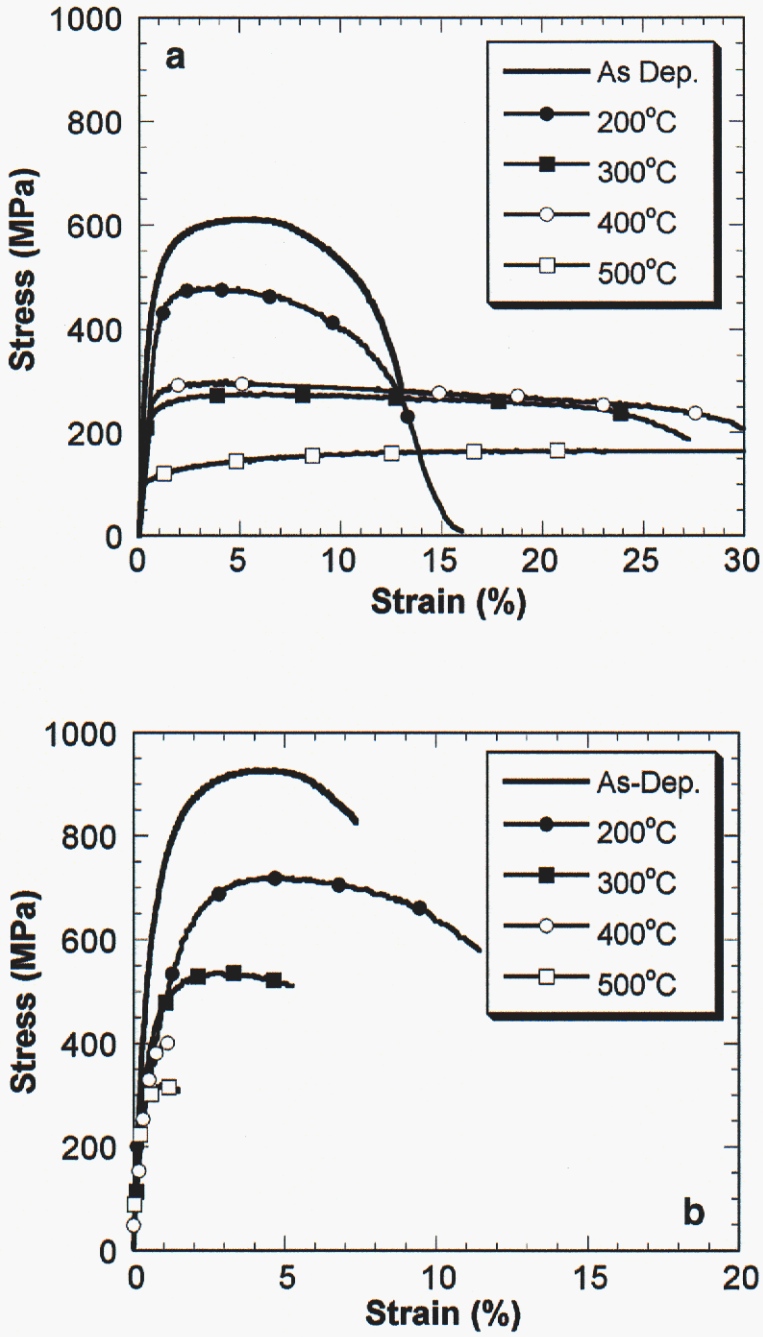

Figure 5. Elevated temperature tensile test results on electrodeposited (a) baseline Ni samples and (b) ODS-Ni.

Table III: Average Elevated Temperature Mechanical Properties

Test Temperature (°C)	Yield Strength (MPa)		UTS (MPa)	
	Baseline	ODS	Baseline	ODS
As-Deposited	410	640	620	960
200	380	550	480	720
300	210	410	275	535
400	220	330	300	405
500	100	300	165	325

Nanoindentation measurements

Figure 6(a) schematically shows the location of a series of nanoindentation measurements performed through the thickness of a high aspect ratio structure. These structures, fabricated from both baseline Ni and ODS-Ni bath chemistries, were 25 μm wide with an aspect ratio of approximately 10:1 (thickness:width). One μm deep nanoindentation experiments were performed along the centerline spaced 25 μm apart and about 25 μm from either end of the structures. Figure 6(b) shows hardness as a function of normalized through thickness location obtained from nanoindentation testing on both baseline Ni and ODS-Ni high aspect ratio structures. These results are compared to averaged data, represented by the gray bands in Figure 6(b), from a series of measurements performed near the center of bulk electrodeposited sections where the hardness values were extremely uniform.

The hardness trace through the high aspect ratio baseline Ni structure coincides with the average bulk measurement, indicating that the through thickness deposit mechanical properties are independent of aspect ratio. Equally important, the hardness measured along the length of the high aspect ratio ODS-Ni deposit is also quite uniform and is nearly the same as that measured for the bulk ODS-Ni (4.23 ± 0.23 GPa vs. 3.93 ± 0.15 GPa). The absence of any significant gradient in hardness suggests that the Al_2O_3 dispersoid deposits uniformly through the thickness of even very high aspect ratio structures. Finally, when comparing hardness values of the two materials, the average bulk hardness of the ODS–Ni is approximately 2.5 GPa higher than that of the baseline Ni, consistent with the observed increase in the measured strength of the dispersion strengthened deposit. Previous work has demonstrated good correlation between nanoindentation hardness measurements and yield strength.[23] Based on those measurements, the current hardness measurements suggest that the yield strength of the ODS-Ni should be between 650-700 MPa, very near the value reported in Table II, 640 MPa. Similarly for the baseline Ni, the hardness values shown in Figure 6 would correspond to a yield strength of approximately 375 - 425 MPa, a range which captures the value reported in Table II, 410 MPa.

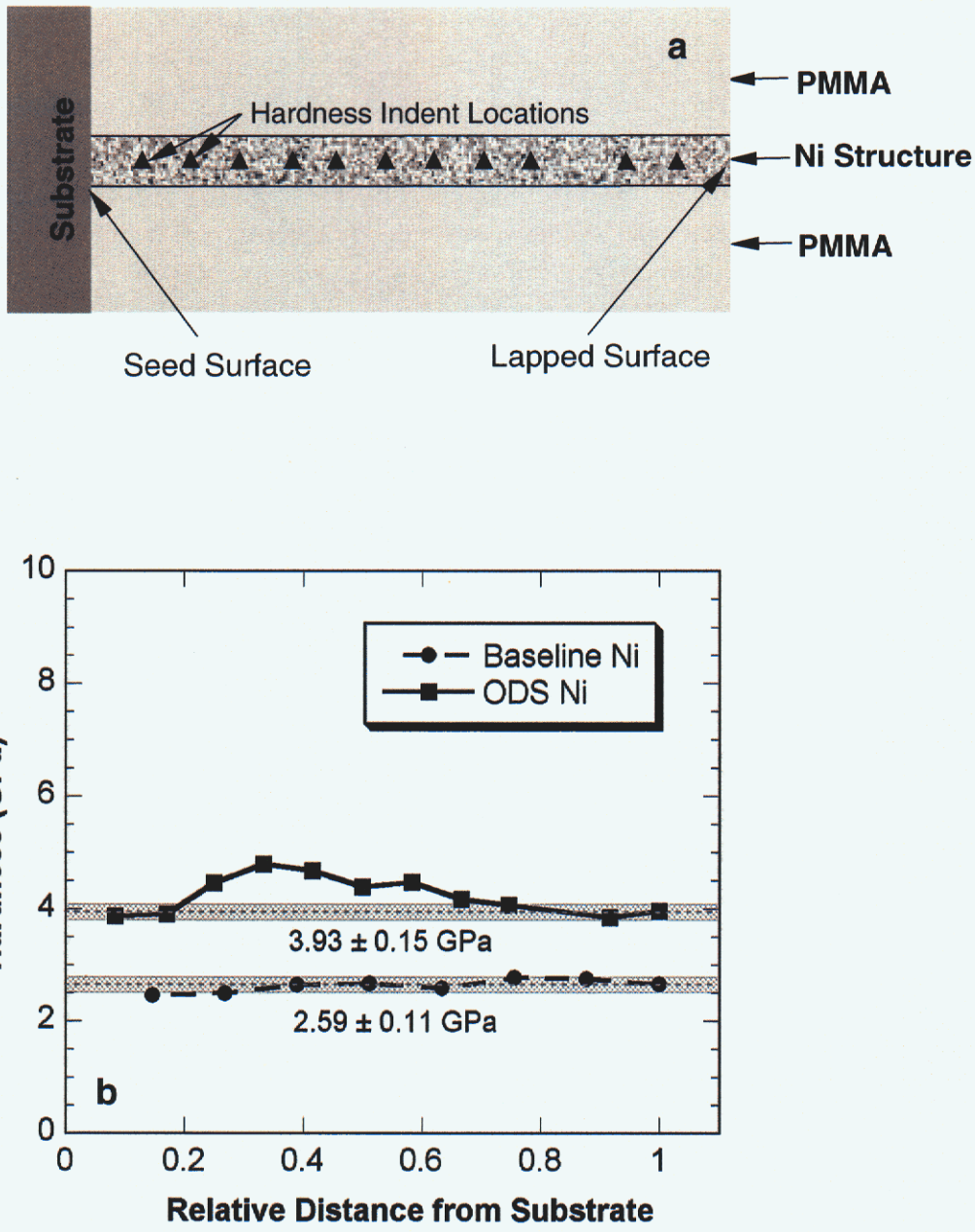

Figure 6. (a) Schematic illustration of nanoindentation experiments in a LIGA-fabricated, high aspect ratio Ni structures. (b) Measured hardness as a function of location in baseline Ni and ODS-Ni cross-section. Locations are referenced from the substrate. Measurements are compared with bulk values of 2.59 ± 0.11 GPa and 3.93 ± 0.15 GPa, determined by averaging a series of indents in low aspect sections of the baseline Ni and ODS-Ni.

Microstructure

A metallographic cross-section imaged using ion beam induced channeling contrast, described in the previous section, of as-deposited baseline nickel electrodeposit is shown in Figure 7(a). The microstructure exhibits the typical columnar grain morphology of nickel electrodeposits fabricated from sulfamate-based bath chemistries with no additives, with the long axis of the grains aligned with the growth direction of the deposit.[7,23] Grain size was measured via the line intercept technique. Transverse to the columnar orientation, the average grain size was found to be 1.3 μm. The columnar length of the grains varied widely with some grains being as long as 30 μm. More typically, the average grain size along the columnar direction was approximately 4 μm. Figure 7(b) shows an ion beam induced channeling contrast image of a metallographic cross-section from a baseline Ni sample after annealing at 600 °C for 1 hour. Heat treating the baseline Ni at this temperature results in a fully recrystallized, equiaxed, coarse grain microstructure. For this sample, the random line intercept method was used to derive an average grain diameter of 11 μm.

Figure 8(a) shows an ion beam induced channeling contrast image of an as-deposited ODS-Ni metallographic cross-section. The orientation of this cross-section is identical, with respect to the plating direction, to that of the baseline Ni micrograph shown in Figure 7(a). The grain size, transverse to the columnar direction, in this image is 0.95 μm, slightly smaller than that for the baseline material. Thus the presence of the suspended particulate in the electrolyte had only a small effect on refining the microstructure of the as-deposited material. Figure 8(a) also reveals the presence of the oxide strengthening agent as very small bright features uniformly distributed throughout the microstructure of the deposit. These features could not be conclusively identified as individual oxide particles or clusters of particles within this image. Figure 8(b) shows a corresponding ion beam induced channeling contrast image of an ODS-Ni specimen after a 600 °C/1hr. heat treatment. In contrast to the baseline electrodeposit, the microstructure has retained its columnar morphology with only slight coarsening. Using the same line intercept method as used for Figure 7(a), the average grain diameter was found to be 1.6 μm. The same bright features are present in this micrograph, indicating that the Al_2O_3 particle distribution was unaffected by the heat treatment.

Figure 9 shows TEM and TEM-based X-ray spectral imaging results indicating that the ~10 nm dia. Al_2O_3 particles tend to agglomerate. Examples of particle clusters are highlighted in the TEM image of a FIB extracted LIGA ODS-Ni section in Figure 9(a). Figure 9(b) shows a high magnification image of a particle cluster in a ODS-Ni sample to better illustrate the nature of the oxide dispersoid clustering. X-ray spectral image analysis [26] was performed on this cluster of particles, and Figures 9(c) and 9(d)

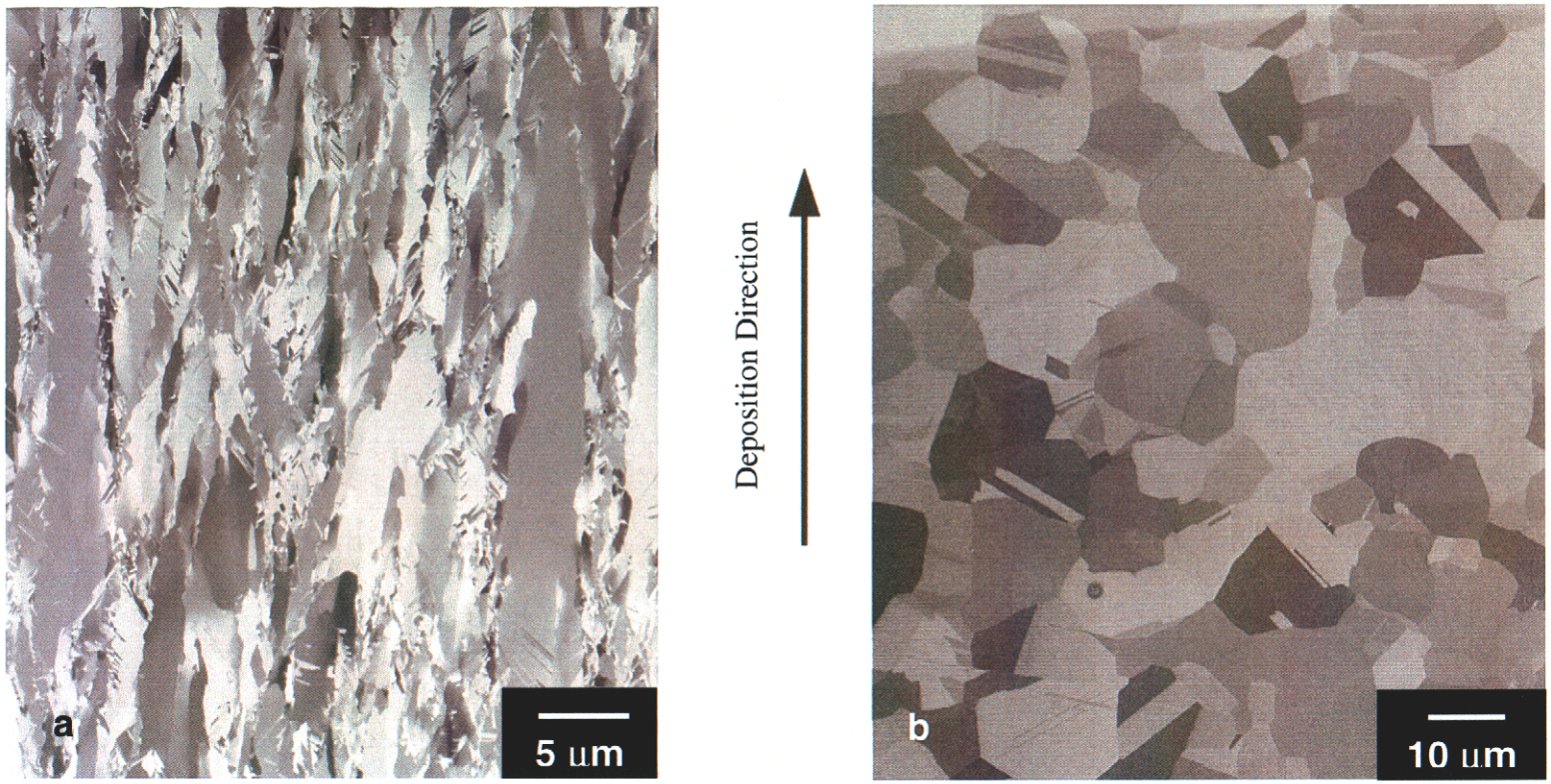

(a) as-deposited baseline Ni

(b) heat treated 600 °C/1 hr baseline Ni

Figure 7. Ion beam induced metallographic cross section images of as-deposited and heat treated 1 hour at 600 °C baseline Ni samples. The as-deposited sample (a) has a columnar microstructure typical of sulfamate bath Ni electrodeposits while the heat treated sample (b) has a coarsened fully recrystallized microstructure typical of pure Ni subjected to intermediate temperature heat treatments.

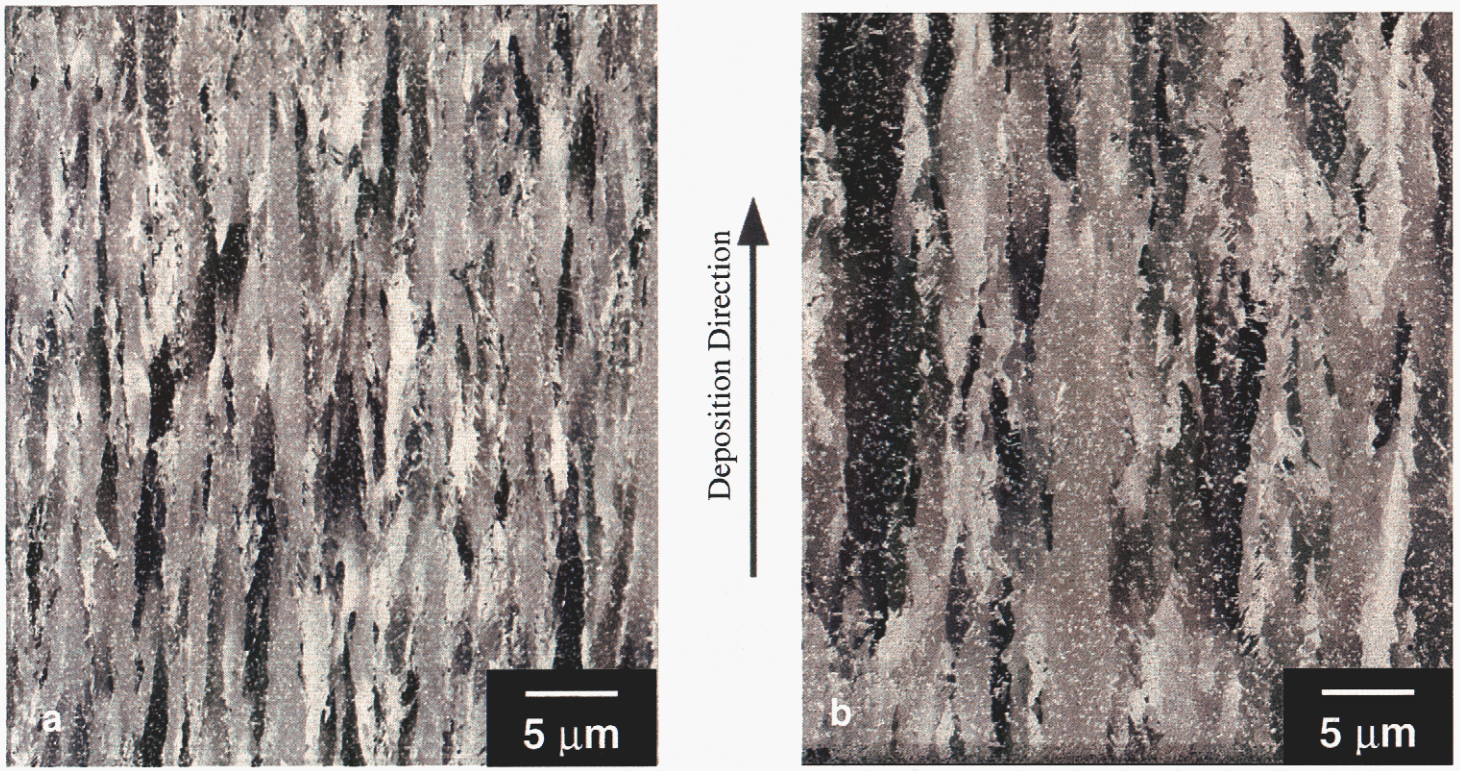

(a) as-deposited ODS-Ni

(b) heat treated 600 °C/1 hr. ODS Ni

Figure 8. Ion beam induced metallographic cross section images of ODS Ni samples (a) as-deposited and (b) heat treated 1 hour at 600 °C. Only slight coarsening of the microstructure resulted from the heat treatment in these samples.

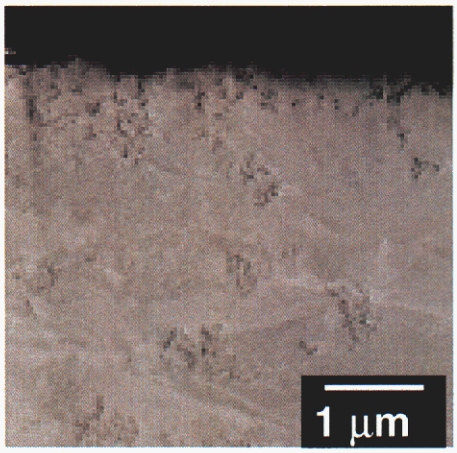

(a) TEM image showing several particulate clusters

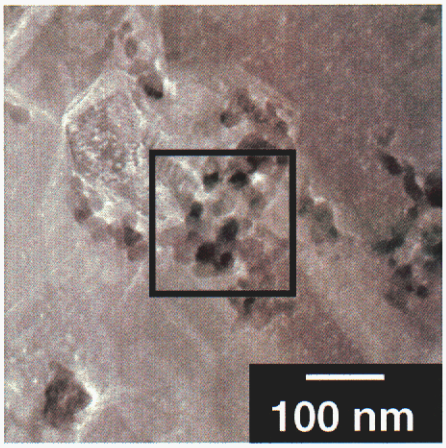

(b) Hi-magnification TEM image of a single particulate cluster

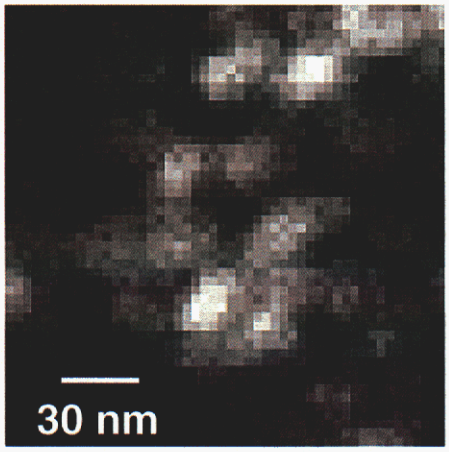

(c) X-ray spectral map of cluster imaged in (b)

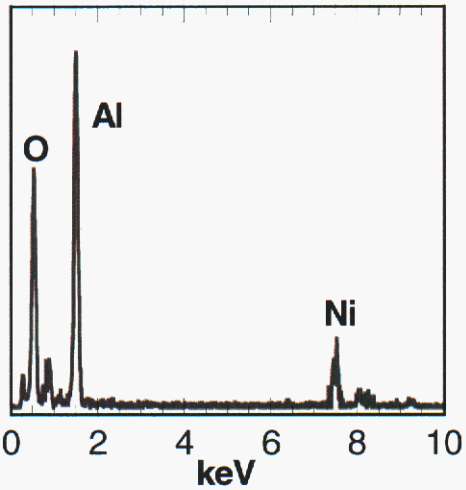

(d) X-ray spectrum identifies principal constituents of cluster particles in (b)

Figure 9. TEM microscopy (a,b) and x-ray spectral imaging (c,d) revealing that Al_2O_3 particulates are clustered into small colonies in the electrodeposited Ni matrix.

summarize the results. A grayscale map of that spectrum's intensity distribution within the area identified in Figure 9(b) is given in Figure 9(c). Within Figure 9(c), white intensity indicates high Al and O concentrations, thus the resultant map verifies a cluster of Al_2O_3 particles. The principal x-ray spectrum identified with the Al_2O_3 particles is given in Figure 9(d). It contains the Al and O peaks with a small Ni residual peak.

Quantitatively determining the volume fraction of the Al_2O_3 particulate in the as-deposited material is difficult, but sufficient information is provided in Figures 8 and 9 to allow for a reasonable estimate. If the particles cluster (as is suggested by Figure 9), equation (2) defines the fraction of the Al_2O_3 particulate within a given cross-sectional area, A_c:

$$V_f \approx A_f = \frac{ns\left(\frac{\pi d^2}{4}\right)}{A_c} \qquad (2)$$

where n is the number of clusters, s is the number of particles per cluster, d is the apparent particle diameter and A_f is the area fraction of particulate as determined by using a 2-D image of the material microstructure. Figure 9 shows a few clusters of particles and, based on this image, a reasonable estimate for the number of particles in a typical cluster is 5-25. The images in Figure 8 and Figure 9(a) allow us to bound the areal density of the particle clusters between about 2 and 10 per μm^2. Assuming a range of cluster sizes between 5-25 particles and a particle diameter of 10 nm, the estimated volume fraction, V_f, of the Al_2O_3 particulate in the ODS-Ni samples lies between 0.001-0.02.

IV. Discussion

Strengthening in baseline Ni

The baseline Ni used in this study exhibits considerably higher yield strength than that found in conventional wrought Ni, where σ_{ys} is usually in the range of 75 –200 MPa.[27] The elevated strength observed in the electrodeposited nickel is thought to be derived from its relatively fine grain size through Hall-Petch considerations. The classical Hall-Petch relationship is given in equation (3):

$$\sigma_{ys} = \sigma_o + kD^{-1/2} \qquad (3)$$

where, σ_0 and k are constants, usually referred to as the frictional stress and the Hall-Petch slope, and D a characteristic grain dimension within a polycrystalline material, usually the average grain diameter. Equation (3) indicates that as the grain size decreases the material strength increases. Assuming dislocation-grain boundary interactions as the basis for Hall-Petch strengthening within a polycrystal, mobile dislocations will most frequently interact with the grain boundaries parallel to the long axes of the grains. Thus, the average transverse grain size is a reasonable characteristic dimension for the columnar microstructures observed in as-deposited LIGA Ni and ODS-Ni samples. The transverse grain dimension of the baseline Ni electrodeposit, given in the previous section, is 1.3 μm [see Figure 6a)], about 5 to 10 times smaller than conventional processed wrought nickel.[27] Eq. (3) indicates this change in characteristic grain dimension results in a two- to three-fold increase in strength of the as-deposited LIGA Ni relative to wrought nickel. This is indeed the case as can be seen by comparing the yield strength of the as-deposited baseline material in Table II to that reported for conventional nickel (75-200 MPa).[27] The microstructure observed in Figure 7(b) further supports the notion that grain size is the principal factor in determining the strength of the pure metal electrodeposit. The grain structure of the 600 °C/1hr. annealed specimen is a fully recrystallized coarser grained equiaxed microstructure. The average grain diameter of this sample, as reported in the previous section, is 11 μm. In concert with microstructure coarsening through grain growth and recrystallization is a precipitous loss in strength, as shown for the baseline Ni in Figure 1(a) and Figure 1(b) and summarized in Table II. From the Hall-Petch relationship, one would expect a drop in the as-deposited yield strength from 410 MPa to 140 MPa after heat treatment which is in very good agreement with the data reported in Table II.

Strengthening of particulate reinforced ODS-Ni

In the as-deposited condition, the ODS-Ni exhibited significantly higher strength than the baseline Ni, however, Figure 8(a) reveals that the grain size of the ODS-Ni is only slightly smaller, approximately 75% that of baseline Ni. Grain refinement and the Hall-Petch relationship can only account for about 15% of the increase in strength (from 410 MPa to 475 MPa) for this change in grain size Thus, the significant additional strengthening in ODS-Ni is not due to the smaller grain size, but rather, due to the presence of the Al_2O_3 dispersion and its interaction with mobile dislocations during plastic deformation. Specifically, the increase in strength is related to the additional stress required to force a dislocation line past an array of rigid obstacles, described phenomenologically by the classical Orowan equation:

$$\Delta\tau = \frac{Gb}{\lambda} \qquad (4)$$

where, G is the shear modulus, b is the burgers vector λ is the inter-obstacle spacing and $\Delta\tau$ is the incremental increase in shear strength imparted by the particles. In the present case, the obstacles of interest are the particle clusters, rather than the individual Al_2O_3 particles themselves. Estimates of particle cluster spacing were made using the images in Figure 8, by counting the number of clusters within a defined area. The clusters are very nearly points in these images; by assuming they are points, a straightforward formula can be derived for determining their spacing in a selected area:

$$\frac{A}{n} = 0.828\lambda^2 \qquad (5)$$

where, A is the area, n is the number of points, and λ is the cluster spacing as before. Estimates of the spacing using this method range from 200 nm to 350 nm. Using equation (2), and assuming G= 76 GPa and b=0.249 nm, standard values for Ni, the estimated increase in $\Delta\tau$, due to the presence of the oxide particles, is approximately 50-100 MPa. This increase in $\Delta\tau$ corresponds to a 150 MPa – 300 MPa increase in yield strength if a Taylor Factor, $M\approx3$ is assumed,[13] in very good agreement with the incremental increase in yield strength of the as-deposited ODS-Ni over its baseline Ni counterpart.

The ODS Ni also showed excellent strength retention subsequent to heat treatment. The origin of this behavior is found in Figure 8(b). The figure reveals that, unlike the baseline Ni, there was only a relatively small change in grain size after the 600 °C heat treatment, presumably the result of grain boundary pinning by the Al_2O_3 dispersoid. The small change in grain size is reflected in the correspondingly small change in the strength of the heat-treated deposit, relative to its as-deposited properties. These observations indicate that the ODS-Ni strength remains governed principally by the Orowan mechanism over the entire range of heat treatments.

The ODS-Ni exhibited superior strength retention at elevated temperatures compared to the baseline Ni. Again, the increase in strength at temperature is likely governed by interactions between the dislocations and the Al_2O_3 particles. In addition to providing barriers to dislocation motion associated with low temperature plastic deformation, the Al_2O_3 particle dispersion, may further act to impede dislocation processes active at higher temperatures such as cross-slip and dislocation creep mechanisms. The loss in ductility however, seems to be an unfortunate consequence of the grain boundary pinning mechanism. Particles or particle clusters present at the pinned grain boundaries act as nucleation sites for deformation-induced grain boundary cavities.[28] This increased tendency for grain boundary cavitation may lead to a decrease in overall ductility in these particulate composite materials.[28-31]

V. Summary

Through-mold, oxide dispersion strengthened nickel (ODS-Ni) electrodeposited samples for mechanical testing and microstructure evaluation were fabricated from a sulfamate bath chemistry using the LIGA process. The oxide dispersion within the samples consisted of 10 nm avg. diameter Al_2O_3 particles distributed throughout the matrix as agglomerated colonies. A study was conducted to compare the microstructure and properties of ODS-Ni samples with baseline Ni samples electrodeposited from an identical bath chemistry without the Al_2O_3 particles.

The ODS-Ni exhibited a 50% increase in as-deposited yield strength relative to the baseline Ni. This increase in strength was attributed to Orowan strengthening, where Al_2O_3 particle colonies acted as barriers to dislocation motion. Investigation of ODS-Ni and baseline Ni samples heat treated up to 600 °C for 1 hour demonstrated that the Al_2O_3 dispersion served to pin grain boundaries, suppressing grain growth during heat treatment, rendering the ODS-Ni resistant to anneal softening. For example, in the case of the 600 °C/1 hr. heat treatment, the yield strength of the ODS-Ni fell by only about 10% while that of the baseline deposit fell by nearly 65%. The high temperature strength of the ODS-Ni was also improved somewhat relative to the baseline Ni-sulfamate. Whereas the baseline Ni suffered a loss in high temperature yield strength of about 75% (410 MPa → 100 MPa), the ODS-Ni exhibited a loss of only approximately 50% (640 MPa → 300 MPa). However, the ductility of the ODS-Ni was severely compromised at the highest test temperature rendering the usefulness of the material problematic for elevated temperature applications.

VI. References

[1] E. Becker, W. Ehrfeld, D. Munchmeyer, H. Betz, A. Hueberger, S. Pontgratz, W. Gashauser, H. J. Michel, and R. von Siemens, Naturwissenschaften, vol. 69 (11), (1982), pp.520-523.

[2] N. Rajan, C. A. Zorman, S. Stefanescu, and T. P. Kicher, Journal of Microelectromechanical Systems, vol.8(3), (1999), pp.251-257.

[3] W. C. Wenzel, and G. Gerlach, Sensors and Actuators, 77, (1999). pp. 14-20

[4] L. Fan, H. Last, R. Wood, B. Dudley, C. Khan Malek, and Z. Ling, Microsystem Technologies , vol. 4 (1998) pp.168-171.

[5] L. T. Romankiw, Electrochimica Acta, vol. 42 (1997) pp. 2985-3005.

[6] S. M. Spearing, Acta Mater. vol. 48 (2000) pp179-196.

[7] W.H. Safrenak, The Properties of Electrodeposited Metals and Alloys, 2nd Ed., American Electroplaters and Surface Finishers Soc., Orlando, FL, 1986. pp. 253-374

[8] W. R. Wearmouth and K. C. Belt, Plat. and Surf. Fin., vol. 66(10) (1979) pp. 53-57.

[9] J. W. Dini, H. R. Johnson and L. A. West, Plat. and Surf. Fin., vol. 65(2) (1978) pp. 36-44.

[10] J.J. Kelly, S.H. Goods and N.Y.C. Yang, Chem. and Sol State Letters, vol. 6(6) (2003), C88-91.

[11] W. B. Stephenson, Jr., *Plating*, vol. 53 (1966) pp. 183-192.

[12] E. Orowan, Dislocations in Metals,. AIME, Warrendale, PA, 1954, p. 69

[13] G. E. Deiter, Mechanical Metallurgy, Mechanical Metallurgy, 2nd ed., McGraw-Hill Book Co., New York, NY, 1976 p. 144

[14] V. P. Greco, Plat. Surf. Finish., vol. 76 (1989) pp.62-67

[15] C. A. Addison and E.C. Kedward, Trans. Inst. Metal Finish, vol. 55, (1977) pp. 41-44

[16] M. Thoma, Plat. Surf. Finish., vol. 71 (1984) pp. 51-53

[17] F.K. Sautter, J. Electrochem. Soc, vol. 110 (1963) pp.557-563

[18] X. M. Ding, N. Merk and B. Ilschner, J. Mater. Sci. vol. 33 (1998) pp.803-809

[19] X.M. Ding, N. Merk and B. Ilschner, J. Chi. Soc. Mech. Engrs. vol. 18 (1997) pp.145-152

[20] J. Foster and B. Cameron, Trans. Inst. Metal Finish, vol. 54 (1976) pp. 178-184

[21] C. White and J. Foster, Trans. Inst. Metal Finish, vol. 59 (1981) pp.8-11

[22] D.T. Schmale, R.J. Bourcier, and T.E. Buchheit, "*Description of a Micro-mechanical Test System*", Report No. SAND97-1608, Sandia National Laboratories, Albuquerque, NM, (1997)

[23] T. E. Buchheit, D. A. LaVan, J.R. Michael, T.R. Christenson and S. E. Leith, Metal Trans. Metal. and Mater. vol. 33A (2002) pp.539-554

[25] J. I. Goldstein et al, Scanning Electron Microscopy and X-ray Microanalysis, Kluwer Academic/Plenum Publishing, New York, 2003, p.558

[25] Phaneuf, M. W., (1999), Micron, vol. 30, pp. 277-288

[26] P.G. Kotula, M.R Keenan and J.R Michael, Microsc. Microanal. vol. 9 (2003) pp. 1-17

[27] Technical Product Specification, *Nickel 200,201 and DURANICKEL alloy 301*, #4M 8-88 IAI-47, Inco Alloys International, Inc., Huntington, WV, 25720, (1988)
[28] S. H. Goods and L.M. Brown, Acta Metall vol. 27 (1979) pp. 1-15
[29] S. H. Goods and W. D. Nix, Acta Metall, vol. 26 (1978) pp.739-752
[30] Flow and Fracture of at Elevated Temperatures, R. Raj (Ed.), American Society for Metals, Metals Park, OH (1985)
[31] H. Reidel, Fracture at High Temperatures, Springer-Verlag, New York, NY, (1986)

VII. Distribution

1	MS 0196	R. Wild, 2618
1	MS 0319	L. L. Lukens, 2618
1	MS 0886	P. G. Kotula, 1822
1	MS 0886	J. R. Michael, 1822
1	MS 0889	J. J. Stephens, 1833
1	MS 0889	J. S. Custer, 1851
1	MS 0889	M. T. Dugger, 1851
1	MS 0889	B.L. Boyce, 1851
1	MS 0889	S. Prasad, 1851
5	MS 0889	T. E. Buchheit, 1851
1	MS 1073	D. W. Peterson,1738
1	MS 1310	C. Vanacek, 2614
1	MS 1310	M. A. Polosky, 2614
1	MS 1415	S. J. Hearn, 1112
1	MS 9405	J. M. Hruby, 8700; Attn:
	MS 9042	C. Moen, 8752
	MS 9161	D. Medlin, 8761
	MS 9401	C. C. Henderson, 8753
	MS-9042	P. Spence, 8774
	MS-9401	J. E Goldsmith, 8751
	MS-9409	W. C. Replogle, 8771
1	MS 9042	S. Griffith, 8752
1	MS 9161	B. Even, 8760
1	MS 9161	D. C. Dibble, 8761
1	MS 9161	E. Marquis, 8761
1	MS 9161	K. E. McCarty, 8761
1	MS 9401	M. Hekmaty, 8751
1	MS 9401	D. Skala,8751
1	MS 9401	A. Talin, 8751
1	MS 9401	G. Aigeldinger, 8753
1	MS 9401	D. R. Boehme, 8753
1	MS 9401	J. T. Ceremuga, 8753
1	MS 9401	J. T. Hachman, 8753
1	MS 9401	D. M.. Heredia, 8753
1	MS 9401	J. J. Kelly, 8753
1	MS 9401	K. Krafcik, 8753
1	MS 9401	D. E. McLean, 8753
1	MS 9401	A. M. Morales, 8753
1	MS 9401	F. J. Pantenburg, 8753
1	MS 9401	T. I. Wallow, 8753
1	MS 9401	P. Yang, 8753

1	MS 9401	G. Lucadamo, 8773
1	MS 9401	S. Spangler,, 08773
1	MS 9401	N. Yang, 08773
1	MS 9402	C. Cadden,8772
1	MS 9402	C. San Marchi, 8772
1	MS 9402	J. Wang, 8773
1	MS 9404	G. D. Kubiak, 8750
1	MS 9405	K. Wilson, 8770
1	MS 9409	J. R. Garcia, 8754
1	MS 9409	W.Y. Lu, 08754
1	MS 9409	S. McFadden, 08754
1	MS 9409	N. Moody, 08754
1	MS 9409	R. Watson, 8754
15	MS 9409	S.H. Goods, 8754
3	MS 9018	Central Technical Files, 8945-1
1	MS 0899	Technical Library, 9616
1	MS 9021	Classification Office, 8511 for Technical Library, MS 0899, 9616 DOE/OSTI via URL

This page intentionally left blank